
Article:
Saad, S.T., Metherell, A.J., Baggaley, E. et al. (1 more author) (2016) Synthesis and photophysical properties of Ir(iii)/Re(i) dyads: control of Ir→Re photoinduced energy transfer. Dalton Transactions, 45 (28). pp. 11568-11579. ISSN 1477-9226

https://doi.org/10.1039/C6DT01614F

Synthesis and photophysical properties of Ir(III)/Re(I) dyads: control of Ir→Re photoinduced energy transfer

Suad T. Saad, Alexander J. Metherell, Elizabeth Baggaley and Michael D. Ward*

Department of Chemistry, University of Sheffield, Sheffield S3 7HF, UK

Email: m.d.ward@sheffield.ac.uk

Abstract

A series of dinuclear Ir(III)/Re(I) complexes has been prepared based on a family of symmetrical bridging ligands containing two bidentate *N,N'*-chelating pyrazolyl-pyridine termini, connected by a central aromatic or aliphatic spacer. The Ir(III) termini are based on $\{Ir(F_2ppy)_2\}^+$ units (where F_2ppy is the cyclometallating anion of a fluorinated phenylpyridine) and the Re(I) termini are based on $\{Re(CO)_3Cl\}$ units. Both types of terminus are luminescent, with the Ir-based unit showing characteristic strong, structured phosphorescence in the blue region (maximum 452 nm) with a triplet excited state energy of 22,200 cm^{-1} and the Re-based unit showing much weaker and lower-energy phosphorescence (maximum 530 nm) with a triplet excited state energy of 21,300 cm^{-1}. The energy gradient between the two excited states allows for partial Ir→Re photoinduced energy-transfer, with substantial (but incomplete) quenching of the higher-energy Ir-based emission component and sensitised emission – evidenced by an obvious grow-in component – on the lower-energy Re-based emission. The Ir→Re energy-transfer rate constants vary over the range 1 – 8 x 10^7 sec^{-1} depending on the bridging ligand: there is no simple correlation between bridging ligand structure and energy-transfer rate, possibly because this will depend substantially on the conformation of these flexible molecules in solution. To test the role of ligand conformation further, we investigated a complex in which the bridging chain is a $(CH_2CH_2O)_6$ unit whose conformation is known to be solvent-polarity dependent, the such chains adopting an open, elongated conformation in water and more compact, folded conformations in organic solvents. There was a clear link between the rate and extent of Ir→Re energy-transfer which reduced in polar solvents as the chain became elongated and the Ir/Re separation was larger; and increased in less polar solvents as the chain adopted a more compact conformation and the Ir/Re separation was reduced.

Introduction

Photoinduced energy-transfer (PEnT) between metal complex units in di- or poly-nuclear assemblies is a phenomenon which has been exploited in many different ways. It has been widely used as a way to funnel excitation energy in a predictable direction from complex units with high energy excited states to those with lower energy states (the 'antenna effect') for applications requiring efficient light harvesting.[1] It is used to achieve a balance between luminescence of different colours from different luminescent centres to make white-light emitting materials.[2] The strong distance dependence of PEnT (whether based on the Förster[3] or Dexter[4] mechanisms) allows it to be used as a sensitive probe of inter-chromophore distance, giving structural information about conformations of flexible molecules and structures of biological assemblies.[5,6] It has also been proposed as a way of transmitting / processing optical information across 'molecular wires' in photonic rather than electronic devices.[7] Amongst the family of d-block complexes with polypyridyl-type ligands, Ru(II)/Os(II) pairs[8] and Ru(II)/Re(I) pairs[9] have received particular attention, as have (more recently) transition metal / lanthanide (d/f) dyads.[10]

As part of our general interest in the study of polynuclear complexes displaying PEnT we have prepared a range of Ir(III) complexes with pendant binding sites that could be used to assemble transition metal / lanthanide dyads.[2a,11-14] These have proven to be of interest for cell imaging[14] and white light generation.[2a] In this paper we report the use of these to prepare Ir(III)/Re(I) dyads in which the relative excited-state energies of the two components mean that the direction of inter-component energy-transfer will be from the Ir(III) unit to the Re(I) unit. A range of different ditopic bridging ligands, containing two chelating pyrazolyl-pyridine termini, has been used. The Ir(III) units, with fluorinated cyclometallated phenylpyridine ligands and a pyridyl-pyrazole unit, show long-lived blue luminescence from the ^{3}MLCT/^{3}LC excited state which is highly characteristic of such luminophores.[2a,12–15] In contrast the {Re(CO)$_3$Cl(diimine)} unit has a lower energy excited state, usually emitting in the red region of the spectrum.[16] Both types of luminophore on their own have been extremely thoroughly studied,[15,16] but they have not been studied in combination in dyads to the best of our knowledge.

Results and Discussion

Synthesis and characterisation.

The complexes prepared are shown in Fig. 1. The following mononuclear Ir(III) complexes and their spectroscopic and luminescence properties have been reported before: Ir•L^{mPh} and Ir•L^{pPh},[11] Ir•L^{naph},[12] and Ir•L^{but}.[13] The other three are new and were prepared by the same general method, by reaction of the appropriate bis(pyrazolyl-pyridine) ligand with dimeric [{Ir(F_2ppy)$_2$}$_2$(μ–Cl)$_2$], with an excess of ligand to minimise formation of the unwanted dinuclear complexes. We wished to have a series of complexes with both aromatic *vs.* aliphatic, and flexible *vs.* rigid, ligand spacers to compare the energy-transfer properties. Crystal structures of two of these, Ir•L^{oPh} and Ir•L^{mTol} (see Table 1 for a summary of crystallographic data, and Table 2 for key structural data) are shown in Figs. 2 and 3. The coordination geometry around the Ir(III) centre is unremarkable with *trans*-pyridyl and *cis*-difluorophenyl donors and a bidentate pyrazolyl-pyridine chelate making up the octahedral coordination; the most interesting feature of the complexes is that in both cases the pendant phenyl ring lies parallel to, and overlapping, with one of the F_2ppy ligands at a distance commensurate with a π-stacking interaction: for example in Ir•L^{oPh} the atoms of the pendant phenyl ring of L^{oPh} are on average 3.38 Å from the mean plane of the adjacent F_2ppy ligand [involving N(11C) and C(26C)].

Conversion of these to the dinuclear Ir/Re complexes was achieved by reaction of each mononuclear Ir(III) complex with Re(CO)$_5$Cl in MeCN, followed by chromatographic purification. For reference purposes for the photophysical studies, the simple Re(I) complex [Re(CO)$_3$Cl(Mepypz)] (Re•L^{Me}) was also prepared. NMR and MS data were consistent with the proposed formulations of these complexes, and examples of crystal structures of four members of the series are in Figs. 5 – 8 (see also Tables 1 and 2). The conformations of the bridging ligands in these complexes are similar to what we observe in the mononuclear Ir complexes, in that the pendant aromatic groups lie stacked in every case with an F_2ppy ligand attached to the Ir(III) ions. Attachment of the {Re(CO)$_3$Cl} unit to the pendant binding site has little effect on this. We showed earlier in a series of Ir(III)/Ln(III) dyads that the electronic coupling that this stacking provides contributed to the efficiency of Dexter Ir→Ln energy transfer; when the

stacking was disrupted for steric reasons the Ir→Ln energy transfer was noticeably less efficient.[2a] We expect that a similar effect could operate in these Ir(III)/Re(I) dyads.

UV/Vis absorption and photophysical properties of the mononuclear complexes.

The UV/Vis absorption spectrum of Ir•L^{oPh}, and the associated steady-state luminescence spectrum, are shown in Fig. 9 (see also Table 3 for a summary of all spectra); these are representative all of mononuclear Ir(III) complexes from this family. The absorption spectra show the usual intense ligand-centred absorptions in the UV region, with the lowest-energy absorption feature at around 360 nm being the LC/MLCT transition responsible for the luminescence. The luminescence spectrum (Fig. 9, inset) is likewise typical and shows the characteristic emission in the blue region of the spectrum, with the most intense emission peak at 455 nm; the clear vibronic structure at lower energy, and small rigidichromism, are characteristic of an excited state with substantial ^{3}LC character based on the F$_2$ppy ligands. In degassed MeCN at room temperature these show lifetimes of around 4 μs (Table 4), which reduces to a few hundred ns in air-equilibrated solvent due to efficient quenching of the ^{3}LC state by dissolved oxygen. The sole exception is for Ir•L^{naph} which (as we reported earlier) is essentially non-luminescent due to quenching of the Ir-based excited state by energy-transfer to the naphthyl-centred triplet state.[12]

For [Re(CO)$_3$Cl(Mepypz)] (Re•L^{Me}) the ^{3}MLCT absorption occurs at 337 nm. The resulting luminescence – a characteristically broad, featureless signal – is at considerably lower energy than in the Ir(III) complexes, with a maximum at 530 nm and a lifetime in degassed MeCN of 245 ns. This luminescence is strongly rigidochromic – a characteristic of the predominantly charge-transfer nature of the excited state – undergoing blue-shifting to 470 nm in a frozen solution at 77K. From the 77K emission maxima of the two types of chromophore we can see that the triplet excited state energies are 22,200 cm^{-1} and 21,300 cm^{-1} for the Ir(III) and Re(I) units respectively, meaning that there is a gradient which should be sufficient for Ir→Re PEnT to occur in the dyads without the back energy-transfer that can occur if the gradient is small. The gradient is however small (≈ 1000 cm^{-1}) which means that, at room temperature, thermally-activated back energy-transfer is possible and Ir→Re PEnT may be incomplete.

Spectroscopic and photophysical properties of dinuclear complexes: Ir-Re energy-transfer.

For the Ir/Re dyads, the increased absorbance in the 300 – 400 nm region compared to the mononuclear Ir complexes arises from the MLCT transition associated with the {$Re(CO)_3Cl$(diimine)} fragment, which occurs at 340 nm for the model complex Re•L^{Me}. This overlaps with the LC/MLCT transition of the Ir(III) units but is not distinctly resolved. It will be clear that overlap of the absorption spectra of the Ir and Re units means that selective excitation of one chromophore is not possible. A representative absorption spectrum, of Ir•$L^{p\text{-}Ph}$•Re, is in Fig. 10(a).

Selected steady-state luminescence spectra of the Ir-Re dyads are shown in Fig. 10(b); they have been normalised so that the highest intensity components of the Ir-based emission signal at 452 nm appear equal. Ir•L^{nap}•Re, the Ir-based emission is quenched by the naphthyl unit.[12] In addition the Re-based luminescence for this complex was very weak to the extent that it was barely detectable and its lifetime could not be measured. As the triplet state of the naphthyl unit (21200 cm^{-1}) is similar in energy to the ^{3}MLCT state of the Re(I) unit, it is possible that the naphthyl triplet state – which is non-luminescent in fluid solution – acts as an energy sink to quench both metal luminophores. Consequently Ir•L^{nap}•Re is not included in the following discussion.

For all other Ir-Re dyads it is clear that the emission spectra contain a combination of both types of emission feature, with the blue end of the spectrum dominated by the structured Ir-based emission, but with a significant shoulder at around 550 nm which extends further into the red region arising from the broad Re-centred emission. The quantum yields of these are low – all *ca.* 0.01 in air-equilibrated MeCN – which is much lower than for the Ir-based emission on its own from the mononuclear complexes, for which quantum yields are typically *ca.* 0.1 under the same conditions.[2a,13]

The observation of two overlapping emission components (Ir-based and Re-based) on its own does not prove anything about the presence or absence of Ir→Re PEnT, because at the excitation wavelength (360 nm) both metal chromophores absorb light; so what we observe is consistent with what would be expected from direct excitation of both chromophores even if they were non-interacting. However the occurrence of Ir→Re PEnT is clear from the substantial quenching of the Ir-based emission intensity in each dyad compared to its mononuclear Ir(III) complex under isoabsorbing conditions. We cannot measure directly quantum yields for the Ir-based

emission components in the dyads, as the Ir-based and Re-based emission components overlap. But time-resolved measurements, in contrast, give a very clear and quantitative way to measure the Ir→Re PEnT and relate it to the structure of the bridging ligands. The energy-transfer should be observable by (i) a reduction in the lifetime of the Ir-based emission, and (ii) a rise-time (grow-in) of the Re-based emission intensity at a rate that matches the Ir-based decay. Accordingly we measured the time-resolved behaviour of the luminescence in the 550 – 600 nm range (using a bandpass filter) which is a region in which the weak Re-based emission component has its maximum intensity, and will not be completely swamped by the Ir-based emission component. Representative traces shown in Fig. 11 clearly depict a short-lived grow-in, whose lifetime varies between complexes, followed by a decay with a lifetime of the order of hundreds of ns in every case.

The initial grow-in corresponds to that part of the Re-based emission intensity which does not arise from direct excitation but which is sensitised by Ir→Re PEnT. It is necessary that this rise-time for Re-based emission matches the Ir-based decay time, and therefore we have an indirect but simple way of determining the residual Ir-based emission lifetimes after partial quenching due to the energy-transfer process (τ_q^{Ir}). This would be difficult to do directly due to overlap between Ir-based and Re-based emission components which might make temporal deconvolution difficult. In addition, because the Ir-based decay is necessarily synchronous with the Re-based rise time, what we observe in the time-resolved decay trace is therefore the superposition of a Re-based grow-in which has a high amplitude at the wavelength range examined, and a lower amplitude Ir-based decay: these are opposite in sign and have not cancelled out, with the former dominating. As the values of τ_q^{Ir} are very much shorter than the unquenched Ir-based emission lifetimes under the same conditions (τ_u^{Ir}, *ca.* 4 μs) we can simply estimate that the energy transfer rate constant to be $k_{EnT} \approx 1/\tau_q^{Ir}$. The values for these are summarised in Table 4 and can be related to the bridging ligand structures and metal-metal separations (which are in Table 2 for the crystallographically characterised examples).

In all cases where there is a single aromatic ring bridge in the ligand, the rise-time of the Re-based emission (and hence the partially-quenched Ir-based decay time which must be equivalent) is around 100 ns, giving an Ir→Re energy-transfer rate of *ca.* 10^7 sec^{-1} in every case. Interestingly however, the saturated bridges in Ir•L^{but}•Re

affords a much shorter rise-times of 13 ns respectively, leading to a faster Ir→Re energy-transfer rate of 8 x 10^7 sec^{-1}. In Ir•L^{but}•Re the bridging ligand provides a short four-atom connection between the two pyrazolyl-pyridine units; but this is the same as in Ir•L^{oPh}•Re for which the energy-transfer rate is nearly an order of magnitude slower. Given the sensitivity of energy-transfer rates to distance, this implies differences in the solution conformations of Ir•L^{but}•Re and Ir•L^{oPh}•Re which afford a shorter Ir•••Re separation in the former case, and indeed the crystal structure of mononuclear Ir•L^{but} indicates a compact conformation in which the two pyrazolyl-pyridine sites lie close together.[13] In all of these cases, fitting the tail of the emission decay showed a lifetime in the region 250 – 400 ns which is entirely consistent with the Re-based emission decay as it matches well what we observed for mononuclear [$Re(CO)_3Cl(L^{Me})$] (245 ns in the same degassed solvent).

Given that the excited states concerned on the Ir(III) and Re(I) units are known to be predominantly of triplet character we would expect the Ir→Re PEnT process to occur predominantly by the Dexter double electron-exchange mechanism.[4] Apart from the well-understood contributions of distance and electronic coupling to this process, it also relies on spectroscopic overlap between the emission spectrum of the donor and the absorption spectrum of the acceptor. Fig. 12 illustrates this and shows how small is the proportion of the Ir-based emission spectrum and the Re-based absorption spectrum that overlap, in the 400 – 450 nm region (highlighted by a blue arrow). This, together with the small gradient between the excited states, explains why the Ir→Re PEnT process is incomplete with the Ir(III) emission not being fully quenched. This contrasts with (for example) numerous Ru(II)/Os(II) dyads in which Ru→Os PEnT is often complete even over substantially greater distances: the typical emission of Ru(II) polypyridyl complexes at around 600 nm provides substantial overlap with the tail end of Os(II)-based absorptions, leading to efficient PEnT.[8]

Attempts to examine Ir→Re energy-transfer rates by measuring lifetimes at 77 K were inconclusive. We could observe a slow emission decay of typically 5 – 10 μs which (by analogy with the discussion above) should be associated with the sensitised Re-based component. However no grow-in feature was detectable even though energy-transfer must still be occurring. This is likely because the short-lived grow-in of sensitised Re-based emission is necessarily synchronous with the short-lived decay of Ir-based emission, and overlap of the two may lead to a situation where the Re-based

rise time is not detectable. We note that the strong blue-shift of the sensitised Re-based emission – see earlier – means that it overlaps much more with the residual Ir-based emission (which is only weakly rigidochromic)[2a] at 77K than it does at RT, so selective time-resolved measurements on the Re-based emission component are no longer possible.

Energy-transfer in a conformationally switchable complex

Given the clear variation in Ir→Re PEnT rates across different ligands, we were interested to see if we could exploit the solvent-dependent conformational changes of a poly(oxo-ethylene) chain[17] to modulate energy-transfer. We demonstrated a while ago that in Ru(II)/Os(II)[18] and Ru(II)/pyrene[19] bichromophoric complexes, in which the two luminophores are connected by a poly(oxo-ethylene) spacer, the solvent-dependent compression (low polarity solvents) and elongation (in more polar solvents) of the chain could be used to alter the inter-chromophore separations in the dyads, with concomitant changes in the energy-transfer rates.[18,19]

Accordingly we prepared the new bridging ligand L^{PEG} by reaction of two equivalents of deprotonated 3-(2-pyridyl)pyrazole with penta(ethyleneglycol)ditosylate to give a bis(pyrazolyl-pyridine) bridging ligand containing a poly(oxoethylene) chain whose conformation is solvent dependent; this was used to prepare mononuclear Ir•L^{PEG} and dinuclear Ir•L^{PEG}•Re using the same methods as for the other complexes. Mononuclear Ir•L^{PEG} gives similar UV/Vis and luminescence behaviour in MeCN to the other complexes. Dinuclear Ir•L^{PEG}•Re likewise shows similar luminescence behaviour in MeCN to the other complexes, with a luminescence spectrum containing both Ir-based and Re-based emission components and a rise-time for the Re-based emission component of 35 ns, indicative of an Ir→Re PEnT rate of 3×10^7 sec^{-1}. This is considerably faster than we observed with a range of aromatic spacers, despite the 18-atom saturated spacer, which strongly implies a folded conformation for Ir•L^{PEG}•Re in which the two termini are in close contact, thereby permitting Dexter-type energy-transfer.

To probe this further we have investigated the photophysical properties of Ir•L^{PEG}•Re in a range of solvents. Fig. 13 shows the dramatic effect of changing solvent on the extent of Ir→Re PEnT as the conformation of the poly(oxoethylene) bridge changes. The spectrum in black is mononuclear Ir•L^{PEG} in MeCN showing just typical Ir-

based emission essentially identical to that in Fig. 9 (inset), *i.e.* with no Re-centred emission component present. The spectrum in red, in contrast, is for Ir•L^{PEG}•Re in CH_2Cl_2. In this case the additional emission at low energy from the broad Re-based emission component (centred at 530 nm) is clear. In this relatively non-polar solvent the poly(oxo-ethylene) chain is expected to adopt a compact, folded conformation which will bring the Ir and Re complex units into close proximity to maximise Ir→Re PEnT. As the solvent polarity is increased by moving to MeCN and then MeOH, and then different amounts of water in MeCN and finally pure water, we can see the steady loss of the sensitised Re-based emission component as the increasing solvent polarity results in opening out of the poly(oxo-ethylene) chain and a reduction in the amount of Ir→Re PEnT.

This was borne out by time-resolved measurements. In MeCN, when the Re-based emission intensity is close to its highest value, we could see a rise-time of 35 ns for the Re-based emission, indicating an Ir→Re PEnT rate of *ca.* 3×10^7 sec^{-1} . However in water no rise-time for the Re-based emission could be detected, indicating that the energy-transfer process no longer occurs because of the greater distance between the Ir(III) and Re(I) termini. Thus, the weak Re-based emission component [the small increase in emission intensity from Ir•L^{PEG}•Re in water (pale blue spectrum in Fig. 12), compared to the purely Ir-based emission (black spectrum in Fig. 13)] arises from direct excitation of the Re-based component: as we showed earlier, both Ir-based and Re-based chromophores absorb at 360 nm, so selective excitation of one over the other is not possible. It follows that the additional Re-based emission component that becomes more apparent as solvent polarity decreases from water (pale blue spectrum) to CH_2Cl_2 (red spectrum) arises from increased Ir→Re PEnT as the flexible bridging ligand becomes more compact and brings the metal termini together. A simple subtraction of the normalised emission spectrum of Ir•L^{PEG} in MeCN (Ir-based emission alone, black in Fig. 12) from that of Ir•L^{PEG}•Re in CH_2Cl_2 (both emission components overlapping) is shown in the inset of Fig. 12 and shows an emission profile that is identical to that of the Re-based emission on its own, with a maximum at 530 nm.

Conclusions

Bis(pyrazolyl-pyridine) ligands provide a convenient way to combine luminscent Ir(III)/phenylpyridine and {$Re(CO)_3Cl$} units in dinuclear complexes in which the

higher-energy excited state of the Ir(III) terminus is partly quenched by photoinduced energy-transfer to the lower-lying excited state of the Re(I) terminus, resulting in appearance of sensitised Re(I)-based luminescence, to an extent that depends on the nature of the bridging ligand. A range of bridging ligands containing a phenyl spacer substituted in different ways afford a rate constant of *ca.* 10^7 sec^{-1} for the Ir→Re energy-transfer, whereas a simple butane-1,4-diyl C_4 chain gives a much faster energy-transfer rate of 8 x 10^7 sec^{-1}. In a conformationally switchable bridging ligand whose termini are separated by a poly(oxo-ethylene) chain, the opening and closing of the chain associated with the change in solvent polarity using a range of solvents and solvent mixtures affords a smooth variation in the extent of Ir→Re energy-transfer associated with changes in metal/metal separation.

Acknowledgements. We thank the Cultural Attaché of the Embassy of the Republic of Iraq for a PhD studentship (to S. T. S.).

Experimental

General details.

Solvents, metal complex precursors and organic reagents were purchased from Sigma Aldrich or Alfa Aesar. The following instrumentation was used for routine spectroscopic characterisation: NMR, Bruker AV-3HD 400 MHz or AV-3HD 500 MHz spectrometers; electrospray mass spectra, and Agilent 6530 QTOF-LC/MS instrument; UV/Vis spectra, a CARY 50 Bio spectrophotometer; luminescence spectra, a Jobin-Yvon FluoroMax 4 spectrofluorimeter. Luminescence lifetimes were was measured using an Edinburgh Instruments 'Mini-τ' instrument using a 405 nm pulsed diode laser excitation source; solutions that were degassed had a stream of argon bubbled through them in a septum cell for 10 minutes.

The following compounds were prepared according to published methods: Ir•L^{mPh} and Ir•L^{pPh};[11] Ir•L^{naph};[12] Ir•L^{but};[13] [{Ir(F_2ppy)$_2$}$_2$(μ–Cl)$_2$];[20] L^{oPh};[21] L^{mTol};[22] and [Re(CO)$_3$Cl(pypzH)] [where pypzH = 3(2-pyridyl)pyrazole].[23]

X-ray crystallography.

Data were collected on a Bruker Apex-II diffractometer equipped with a sealed-tube source (Mo-Kα radiation). In each case a crystal was removed from the mother liquor, coated with oil, and transferred rapidly to a stream of cold N_2 on the diffractometer to prevent any decomposition due to solvent loss. In all cases, after integration of the raw data, and before merging, an empirical absorption correction was applied (SADABS)[24] based on comparison of multiple symmetry-equivalent measurements. The structures were solved by direct methods and refined by full-matrix least squares on weighted F^2 values for all reflections using the SHELX suite of programs.[25] Pertinent crystallographic data are collected in Table 1, and metal coordination sphere bond distances are collected in Table 2. For [Ir(F_2ppy)$_2$(L^{pPh}) Re(CO)$_3$Cl](NO$_3$)•MeCN the SQUEEZE function in PLATON[26] was required to remove some residual electron density which could not be modelled and is p[resumed to arise form severely disordered solvent molecules. This corresponds to 188 electrons per unit cell: as the crystals were grown from MeCN/Et_2O this could be ascribed to approximately 2 MeCN molecules or one ether molecule per complex unit.

Syntheses of new bridging ligand L^{PEG}.

A mixture of 3-(2-pyridyl)pyrazole (0.245 g, 1.69 mmol) and sodium hydride (60% dispersion in mineral oil: 0.067g, 1.69 mmol) in dry THF (40 cm^3) was stirred for 15 minutes under N_2. To this was added a solution of hexaethyleneglycol ditosylate (0.5 g, 0.85 mmol) in dry THF (6 cm^3) and the mixture was heated to reflux for 1h. After filtration and evaporation of solvent, the residue was purified by column chromatography on alumina (Brockmann activity III) *via* gradient elution, initially using ethyl acetate/hexane (60:40 *v/v* to 80:20 *v/v*) followed by ethyl acetate/MeOH (99:1 *v/v*) to give the pure ligand in 72% yield. ^{1}H NMR (400 MHz, CD_3CN): δ(ppm) 8.62 (2H, d, *J* 4.9); 7.89 (2H, d, *J* 8.0); 7.70 (2H, ddd, *J* 1.5, 5.5, 7.1); 7.58 (2H, d, *J* 1.8); 7.20-7.16 (2H, m); 6.84 (2H, d, *J* 1.8); 4.37 (4H, t, *J* 5.3), 3.88 (4H, t, *J* 5.2); 3.59 (16H, d, *J* 8.9 Hz). ESMS: *m/z* 537.3 $(M + H)^+$, 269.1 $(M + 2H)^{2+}$

Syntheses of mononuclear Ir(III) complexes.

The new mononuclear Ir(III) complexes Ir•L^{oPh}, Ir•L^{mTol} and Ir•L^{PEG} were prepared in exactly the same way as the previously-reported Ir(III) complexes,[11-13] by reaction of $[\{Ir(F_2ppy)_2\}_2(\mu\text{–}Cl)_2]$ with an excess of the relevant bridging ligand, followed by chromatographic purification. Characterisation data are as follows.

Data for $[Ir(F_2ppy)_2(L^{o\text{-}ph})]NO_3$ (Ir•L^{oPh}). Yield: 50% . ^{1}H NMR (400 MHz, CD_3CN): δ(ppm) 8. 56 (1H, d, *J* 5.7); 8.31 (2H, t, *J* 10.1); 8.13 (1H, td, *J* 1.4, 7.8); 8.00 (1H, d, *J* 2.8); 7.98 – 7.90 (2H, m); 7.86 (1H, d, *J* 5.7); 7.80 – 7.73 (4H, m); 7.62 (1H, d, *J* 5.9), 7.56 (1H, d, *J* 2.4); 7.42 (1H, d, *J* 2.7); 7.39 (1H, m); 7.29 – 7.21 (2H, m); 7.14 – 7.07 (2H, m); 7.02 (1H, d, *J* 7.3); 6.86 (1H, d, *J* 2.2); 6.73 – 6.58 (3H, m); 5.82 (1H, dd, *J* 2.3, 8.4); 5.64 (1H, d, *J* 17.1); 5.46 (1H, dd, *J* 2.3, 8.7); 5.41 (1H, d, *J* 8.1); 5.28 (1H, d, *J* 17.1 Hz); 4.73 (2H, m). ESMS: *m/z* 965 $(M - NO_3)^+$, 483$(M - NO_3 + H)^{2+}$. Found: C, 51.5; H, 3.8; N, 11.3%. Calculated for for $C_{46}H_{32}IrF_4N_9O_3\bullet 3H_2O$: C, 51.1; H, 3.5; N, 11.7%.

Data for $[Ir(F_2ppy)_2(L^{mTol})]NO_3$ (Ir•L^{mTol}). Yield: 52% . ^{1}H NMR (400 MHz, CD_3CN): δ(ppm) 8.59 (1H, d, *J* 4.1); 8.26 (1H, d, *J* 8.3); 8.16 (1H, dt, *J* 1.4, 8.9); 8.06 (1H, td, *J* 1.6, 7.9); 7.96 (1H, d, *J* 2.9); 7.91 (1H, ddd, *J* 1.4, 7.8, 8.6), 7.83 (1H, dt, *J* 1.2, 1.0), 7.79 (2H, dd, *J* 1.0, 5.2); 7.76 – 7.69 (2H, m); 7.62 (1H, dd, *J* 1.0, 5.9); 7.57 (1H, dt, *J* 1.3, 5.9), 7.54 (1H, d, *J* 2.5); 7.36 (1H, ddd, *J* 7.3, 5.6, 1.4); 7.29 – 7.25 (2H, m); 7.20 – 7.12 (2H, m); 6.85 (2H, d, *J* 2.5); 6.71 – 6.60 (2H, m); 5.77 (1H, s); 5.68 (1H, dd, *J* 2.3, 8.6); 5.53 (1H, s); 5.48 (1H, dd, *J* 2.5, 3.5 Hz); 5.25 – 4.95 (4H, m); 2.07 (3H, s). ESMS: *m/z* 979 $(M - NO_3)^+$,

490 (M – NO_3 + H)$^{2+}$. Found: C, 51.5; H, 3.5; N, 11.4%. Calculated for $C_{47}H_{34}IrF_4N_9O_3$•$3H_2O$: C, 51.5; H, 3.7; N, 11.5%.

Data for [Ir(F_2ppy)$_2$(L^{PEG})]NO_3 (Ir•L^{PEG}). Yield: 21% . ^{1}H NMR (400 MHz, CD_3CN): δ(ppm) 8. 54 (1H, d, *J* 4.9); 8.37 (1H, d, *J* 8.3); 8.30 (1H, d, *J* 8.3); 8.21 (1H, td, *J* 7.7, 1.2); 8.06(1H, td, *J* 8.1, 1.6); 8.00 – 7.90 (4H, m); 7.77 (1H, m); 7.76 – 7.72 (2H, m); 7.66 (1H, d, *J* 5.9); 7.63 (1H, d, *J* 2.3); 7.35 (1H, ddd, *J* 6.8, 5.5, 1.2); 7.25 – 7.21 (2H, m); 7.20 – 7.12 (2H, m); 6.80 (1H, d, *J* 2.2); 6.76 – 6.63 (2H, m); 5.77 (1H, dd, *J* 2.4, 8.7); 5.62 (1H, dd, *J* 11.0, 2.4); 4.31 (2H, t, *J* 5.4 Hz); 3.87 – 3.74 (4H, m); 3.56 – 3.22 (18H, m). ESMS: *m/z* 1109 (M – NO_3)$^+$, 555 (M – NO_3 + H)$^{2+}$. Found: C, 51.0; H, 5.0; N, 9.5%. Calculated for $C_{50}H_{48}IrF_4N_9O_8$•$4H_2O$: C, 50.8; H, 4.8; N, 9.5%.

Synthesis of dinuclear Ir(III)/Re(I) complexes.

A mixture of the appropriate mononuclear Ir(III) complex (0.1 mmol) and $Re(CO)_5Cl$ (43 mg, 0.12 mmol) in MeCN (20 cm^3) was heated to reflux overnight under N_2 and in the dark. After cooling, the solvent was removed by evaporation, and the residue was dissolved in CH_2Cl_2 (20 cm^3) and shaken three times with saturated aqueous KPF_6 (20 cm^3). The organic layer was separated and dried over $MgSO_4$. Evaporation of the solvent afforded the crude product which was purified by silica column chromatography using MeCN / saturated aqueous KNO_3 (98:2, v/v) as eluent. Evaporation of solvents afforded a solid residue from which excess of KNO_3 was removed by extraction of the pure dinuclear complex with CH_2Cl_2 and evaporation to dryness.

Data for [Ir(F_2ppy)$_2$(L^{but})Re$(CO)_3Cl$]NO_3 (Ir•L^{but}•Re). Yield: 61% . ^{1}H NMR (400 MHz, CD_3CN): δ(ppm) 8.91 (1H, d, *J* 5.4); 8.37 (1H, dd, *J* 8.4, 17.1), 8.29 (1H, t, *J* 8.4), 8.22 – 8.03 (4H, m); 7.99 – 7.84 (3H, m); 7.79 – 7.74 (2H, m); 7.67 – 7.60 (2H, m); 7.55 – 7.49 (1H, m); 7.37 – 7.31 (1H, m); 7.22 (1H, dd, *J* 2.8, 5.9); 7.17 (0.5H, t, *J* 7.2); 7.09 – 7.01 (2H, m); 6.99 (0.5H, t, *J* 6.7); 6.75 – 6.65 (2H, m); 5.82 (0.5H, dd, *J* 2.2, 8.5), 5.76 (0.5H, dd, *J* 2.2, 8.5); 5.57 (1H, td, *J* 2.2, 8.5 Hz); 4.35 – 4.14 (2H, m); 3.75 – 3.68 (2H, m); 1.69-1.14 (2H, m); 1.40 – 1.30 (2H, m). ESMS: *m/z* 1223 (M – NO_3)$^+$. This complex failed to yield reliable and repeatable elemental analytical data because it is slightly hygroscopic.

Data for [Ir(F_2ppy)$_2$(L^{naph})Re$(CO)_3Cl$]NO_3 (Ir•L^{naph}•Re). Yield: 67% . ^{1}H NMR (400 MHz, CD_3CN): δ(ppm) 8.99 (1H, m); 8.33 (1H, d, *J* 7.9); 8.28 (1H, d, *J* 8.3), 8.22 – 8.09 (4H, m); 7.96 (1H, t, *J* 7.9); 7.85 – 7.74 (4H, m); 7.68 – 7.54 (3H, m); 7.46 (1H, d, *J* 2.8 Hz); 7.44

– 7.33 (3H, m); 7.32 – 7.17 (4H, m); 7.07 (1H, m); 6.73 (1H, m); 6.65 (1H, m); 6.24 – 6.07 (2H, m); 5.92 – 5.79 (2H, m); 5.68 – 5.59 (2H, m); 5.47 – 5.33 (2H, m). ESMS: *m/z* 1321 $(M - NO_3)^+$. Found: C, 44.8; H, 3.1; N, 8.5%. Calculated for $C_{53}H_{34}IrReClF_4N_9O_6 \bullet 2H_2O$: C, 44.9; H, 2.7; N, 8.9%.

Data for $[Ir(F_2ppy)_2(L^{mTol})Re(CO)_3Cl]NO_3$ (Ir•L^{mTol}•Re). Yield: 87% . ^{1}H NMR (400 MHz, CD_3CN): δ(ppm) 8.91 (1H, m); 8.29 (2H, m); 8.20 – 8.10 (3H, m); 7.96 – 7.88 (2H, m); 7.86 – 7.73 (4H, m); 7.68 – 7.59 (2H, m); 7.57 –7.50 (1H, m); 7.42 – 7.37 (1H, m); 7.35 (0.5H, d, *J* 2.8); 7.27 (0.5H, d, *J* 2.8); 7.20 – 7.10 (3H, m); 6.93 (0.5H, s); 6.86 (0.5H, s); 6.73 – 6.58 (2H, m); 5.84 – 5.65 (3H, m); 5.48 (1H, dd, *J* 2.2, 8.6 Hz); 5.42 – 5.32 (1.5H, m); 5.25 – 5.16 (1.5H, m); 5.02 – 4.91 (1H, m); 2.05 (3H, s). ESMS: *m/z* 1285 $(M - NO_3)^+$. Found: C, 41.9; H, 2.9; N, 8.4%. Calculated for $C_{50}H_{34}IrReClF_4N_9O_6 \bullet 4H_2O$: C, 42.3; H, 3.0; N, 8.9%.

Data for $[Ir(F_2ppy)_2(L^{pPh})Re(CO)_3Cl]NO_3$. Yield: 80% . ^{1}H NMR (400 MHz, CD_3CN): δ(ppm) 8.94 (1H, d, *J* 5.5); 8.30 – 8.25 (2H, m); 8.19 – 8.07 (3H, m); 7.99 – 7.89 (3H, m); 7.83 – 7.69 (3H, m); 7.68 – 7.62 (1H, m); 7.58 – 7.52 (2H, m); 7.40 – 7.34 (2H, m); 7.24 (1H, d, *J* 2.6), 7.21 – 7.14 (1H, m), 7.07 – 7.01 (1H, m); 6.98 – 6.91 (2H, m); 6.72 – 6.65 (1H, m); 6.58 – 6.50 (1H, m); 6.08 – 6.03 (2H, m); 5.72 – 5.60 (2H, m); 5.60 – 5.50 (1H, m); 5.49 – 5.43 (1H, m); 5.30 (1H, d, *J* 17.5); 5.06 (1H, d, *J* 17.5 Hz). ESMS: *m/z* 1271 $(M - NO_3)^+$. Found: C, 43.1; H, 2.9; N, 9.4%. Calculated for $C_{49}H_{32}IrReClF_4N_9O_6 \bullet 2H_2O$: C, 42.9; H, 2.7; N, 9.2%.

Data for $[Ir(F_2ppy)_2(L^{oPh})Re(CO)_3Cl]NO_3$. Yield: 80% . ^{1}H NMR (400 MHz, CD_3CN): δ(ppm) 8.93 (0.5H, dt, *J* 5.4, 1.1); 8.91 (0.5H, dt, *J* 5.4, 1.1); 8.34 – 8.28 (2H, m); 8.19 – 8.11 (3H, m); 8.00 – 7.90 (2H, m); 7.89 –7.78 (3.5H, m); 7.72 (0.5H, d, *J* 2.8); 7.69 (0.5H, d, *J* 2.9); 7.66 (0.5H, d, *J* 5.5); 7.63 (0.5H, d, *J* 5.9); 7.62 (0.5H, d, *J* 2.9); 7.57 – 7.52 (1H, m); 7.44 –7.39 (1.5H, m); 7.37 (0.5H, d, *J* 2.9); 7.29 – 7.11 (4H, m); 6.90 (0.5H, d, *J* 7.7), 6.79 (0.5H, t, *J* 7.6), 6.74 – 6.63 (2H, m); 6.62 – 6.54 (1H, m); 5.77 (1H, dd, *J* 2.1, 8.8), 5.60 (0.5H, d, *J* 7.7 Hz), 5.53 – 5.37 (2.5H, m); 5.32 – 5.12 (1.5H, m); 5.08 – 4.88 (1.5H, m). ESMS: *m/z* 1271 $(M - NO_3)^+$. Found: C, 42.7; H, 3.0; N, 8.8%. Calculated for $C_{49}H_{32}IrReClF_4N_9O_6 \bullet 2H_2O$: C, 43.0; H, 2.7; N, 9.2%.

Data for $[Ir(F_2ppy)_2(L^{m\text{-}Ph})Re(CO)_3Cl]NO_3$. Yield: 67% . ^{1}H NMR (400 MHz, CD_3CN): δ(ppm) 8.91 (1H, m); 8.34 – 8.26 (2H, m); 8.19 – 8.10 (3H, m); 7.96 –7.89 (2H, m); 7.86 (1H, t, *J* 2.9); 7.84 –7.74 (3H, m); 7.67 (0.5H, d, *J* 5.6); 7.65 – 7.60 (1.5H, m); 7.57 – 7.48 (1H, m); 7.42 – 7.37 (1H, m); 7.35 (0.5H, d, *J* 2.8); 7.26 (0.5H, d, *J* 2.8); 7.21 – 7.09

(3.5H, m); 7.06 – 6.96 (1.5H, m), 6.73 – 6.65 (1H, m), 6.64 – 6.55 (1H, m), 6.05 (0.5H, d, *J* 7.1); 5.99 (0.5H, d, *J* 7.6 Hz); 5.94 (0.5H, s); 5.81 (0.5H, s); 5.71 (1H, m); 5.52 – 5.37 (2.5H, m); 5.29 – 5.16 (1.5H, m); 5.03 – 4.90 (1H, m). ESMS: *m/z* 1271 $(M - NO_3)^+$. Found: C, 44.3; H, 2.7; N, 9.5%. Calculated for $C_{49}H_{32}IrReClF_4N_9O_6$: C, 44.2; H, 2.4; N, 9.5%.

Data for $[Ir(F_2ppy)_2(L^{PEG})Re(CO)_3Cl]NO_3$ (Ir•L^{PEG}•Re). Yield: 27% . ^{1}H NMR (400 MHz, CD_3CN): δ(ppm) 8.93 (1H, d, *J* 5.6); 8.37 (1H, d, *J* 8.7); 8.31 (1H, d, *J* 8.5); 8.23(1H, d, *J* 8.1); 8.14 – 8.05 (3H, m); 8.00 – 7.90 (4H, m); 7.79 (1H, d, *J* 5.4), 7.74 (1H, d, *J* 5.9); 7.65 (1H, d, *J* 5.5); 7.51 (1H, ddd, *J* 7.3, 5.5, 1.7), 7.39 – 7.34 (1H, m); 7.23 (1H, d, *J* 2.7); 7.20 (1H, ddd, *J* 7.4, 5.8, 1.5); 7.17 – 7.12 (1H, m); 7.05 (1H, d, *J* 2.8); 6.76 – 6.63 (2H, m); 5.77 (1H, dd, *J* 10.5, 2.3); 5.62 (1H, dd, *J* 10.8, 2.2); 4.65 – 4.53 (2H, m); 4.11 (1H, ddd, J 11.2, 7.1, 4.1 Hz); 4.00 – 3.94 (1H, m); 3.89 – 3.74 (2H, m); 3.63 – 3.22 (18H, m). ESMS*: m/z* 1416 $(M - NO_3)^+$. Found: C, 40.6; H, 3.4; N, 8.5%. Calculated for $C_{53}H_{48}IrReClF_4N_9O_{11}$ •$4H_2O$: C, 41.1; H, 3.6; N, 8.1%.

Synthesis of Re(I) complex [Re(CO)$_3$Cl(Mepypz)] (Re•L^{Me})

A mixture of $[Re(CO)_3Cl(pypzH)]$ (0.030 g, 67 μmol), Cs_2CO_3 (0.32 g, 0.98 mmol), MeI (0.4 cm^3, 1.5 mmol) in MeCN (20 cm^3) was heated to reflux for 2d, after which time the solution was filtered and solvents removed by evaporation. The residue was crystallised from CH_2Cl_2 / hexane to give the product in 55% yield. ^{1}H NMR (400 MHz, CD_3CN): δ(ppm) 8.93 (1H, dt, *J* 1.2); 8.15 – 8.05 (2H, m); 7.85 (1H, d, *J* 2.8); 7.51 (1H, ddd, *J* 7.5, 5.8, 1.6); 7.04 (1H, d, *J* 2.7 Hz); 4.14 (3H, s). ESMS: *m/z* 430 $(M - Cl)^+$. Found: C, 30.7; H, 1.9; N, 9.2%. Calculated for $C_{12}H_9N_3O_3ReCl$: C, 31.0; H, 2.0; N, 9.0%.

References

1 (a) C. A. Bignozzi, R. Argazzi and C. J. Kleverlaan, *Chem. Soc. Rev.,* 2000, **29**, 87; (b) W. M. Campbell, A. K. Burrell, D. L. Officer and K. W. Jolley, *Coord. Chem. Rev.,* 2004, **248**, 1363; (c) J. Baffreau, S. Leroy-Lhez, N. Van Anh, R. M. Williams and P. Hudhomme, *Chem. Eur. J.,* 2008, **14**, 4974; (d) A. Harriman, L. Mallon and R. Ziessel, *Chem. Eur. J.,* 2008, **14**, 11461; (e) T. S. Balaban, N. Berova, C. M. Drain, R. Hauschild, X. F. Huang, H. Kalt, S. Lebedkin, J.-M. Lehn, F. Nifaitis, G. Pescitelli, V. I, Prokhorenko, G. Riedel, G. Smeureanu and J. Zeller, *Chem. Eur. J.,* 2007, **13**, 8411; (f) D. M. Guldi, *Chem. Soc. Rev.,* 2002, **31**, 22; (g) V. Balzani, P. Ceroni, A. Juris, M. Venturi, S. Campagna, F. Puntoriero and S. Serroni, *Coord. Chem. Rev.,* 2001, **219**, 545.

2 (a) D. Sykes, I. S. Tidmarsh, A. Barbieri, I. V. Sazanovich, J. A. Weinstein and M. D. Ward, *Inorg. Chem.,* 2011, **50**, 11323; (b) A. H. Shelton, I. V. Sazanovich, J. A. Weinstein and M. D. Ward, *Chem. Commun.,* 2012, **48**, 2749; (c) P. Coppo, M. Duati, V. N. Kozhevnikov, J. W. Hofstraat and L. De Cola, *Angew. Chem., Int. Ed.,* 2005, **44**, 1806; (d) O. M. ten Kate, R. J. Xie, S. Funahashi, T. Yakeda and N. Hirosaki, *RSC Adv.,* 2016, **6**, 20681; (e) F. de J. Trindade, E. R. Triboni, B. Castanheira and S. Brochsztain, *J. Phys. Chem. C,* 2015, **119**, 26989; (f) F. Kang, Y. Zhang and M. Peng, *Inorg. Chem.,* 2015, **54**, 1462.

3 Th. Förster, *Discuss. Faraday Soc.,* 1959, **27**, 7

4 D. L. Dexter, *J. Chem. Phys.,* 1953, **21**, 836.

5 Reviews: (a) N. Hildebrandt, K. D. Wegner and R. W. Algar, *Coord. Chem. Rev.,* 2014, **273**, 125; (b) S. Preus and L. M. Wilhelmsson, *ChemBioChem,* 2012, **13**, 1990; (c) B. Prevo and E. J. G. Peterman, *Chem. Soc. Rev.,* 2014, **33**, 1144; (d) S. Hohng, S. Lee, J. Lee and M. H. Jo, *Chem. Soc. Rev.,* 2014, **43**, 1007; (e) R. B. Sekar and A. Perlasamy, *J. Cell Biol.,* 2003, **160**, 629; (f) C. Joo, H. Balci, Y. Ishitsuka, C. Buranachai and T. Ha, *Ann. Rev. Biochem.,* 2008, **77**, 51.

6 Specific examples: (a) G. Rahamim, M. Chemerovski-Glikman, S. Rahimipour, D. Amir and E. Haas, *PLoS One,* 2015, **10**, e0143732; (b) T. Heyduk, *Curr. Opin. Biotechnol.,* 2002, **13**, 292; (c) S. J. A. Pope, C. R. Rice, M. D. Ward, A. F. Morales, G. Accorsi, N. Armaroli and F. Barigelletti, *J. Chem. Soc., Dalton Trans.,* 2001, 3025; (d) J. A. Hanson, J. Brokaw, C. C. Hayden, J.-W. Chu and H. Yang, *Chem. Phys.,* 2012, **396**,

61; (e) S. Sindbert, S. Kalinin, N. Hien, A. Kienzler, L. Clima, W. Bannwarth, B. Appel, S. Muller and C. A. M. Seidel, *J. Am. Chem. Soc.,* 2011, **133**, 2463; (f) R. B. Best, K. A. Merchant, I. V. Gopich, B. Schuler, A. Bax and W. A. Eaton, *Prof. Natl. Acad. Sci. USA,* 2007, **104**, 18964;

7 (a) G. Melina and B. Albinsson, *Chem. Soc. Rev.,* 2015, **44**, 845; (b) F. Barigelletti and L. Flamigni, *Chem. Soc. Rev.,* 2000, **29**, 1; (c) R. Ziessel, M. Hissler, A. El-Ghayoury and A. Harriman, *Coord. Chem. Rev.,* 1998, **178**, 1251; (d) B. Albinsson and J. Martensson, *J. Photochem. Photobiol.,* 2008, **9**, 138.

8 (a) J.-P. Sauvage, J.-P. Collin, J.-C. Chambron, S. Guillerez, C. Coudret, V. Balzani, F. Barigelletti, L. De Cola and L. Flamigni, *Chem. Rev.,* 1994, **94**, 993; (b) L. De Cola and P. Belser, *Coord. Chem. Rev.,* 1998, **177**, 301; (c) S. Encinas, L. Flamigni, F. Barigelletti, E. C. Constable, C. E. Housecroft, E. R. Schofield, E. Figgemeier, D. Fenske, M. Neuburger, J. G. Vos and M. Zehnder, *Chem. Eur. J.,* 2002, **8**, 137; (d) H. B. Baudin, J. Davidsson, S. Serroni, A. Juris, V. Balzani, S. Campagna and L. Hammarstrom, *J. Phys. Chem. A,* 2002, **106**, 4312.

9 (a) M. Velayudham and S. Rajagopal, *Inorg. Chim. Acta,* 2009, **362**, 5073; (b) A. Coleman, C. Brennan, J. G. Vos and M. T. Pryce, *Coord. Chem. Rev.,* 2008, **252**, 2585; (c) T. Lazarides, A. Barbieri, C. Sabatini, F. Barigelletti, H. Adams and M. D. Ward, *Inorg. Chim. Acta,* 2007, **360**, 814; (d) R. L. Cleary, K. J. Byrom, D. A. Bardwell, J. C. Jeffery, M. D. Ward, G. Calogero, N. Armaroli, L. Flamigni and F. Barigelletti, *Inorg. Chem.,* 1997, **36**, 2601; (e) D. A. Bardwell, F. Barigelletti, R. L. Cleary, L. Flamigni, M. Guardigli, J. C. Jeffery and M. D. Ward, *Inorg. Chem.,* 1995, **34**, 2438; (f) S. van Wallandael, M. W. Perkovic and D. P. Rillema, *Inorg. Chim. Acta,* 1993, **213**, 253; (g) K. Kalyanasundaram, M. Grätzel and M. K. Nazeeruddin, *Inorg. Chem.,* 1992, **31**, 5243; (h) M. Furue, M. Naiki, Y. Kanematsu, T. Kushida and M. Kamachi, *Coord. Chem. Rev.,* 1991, **111**, 221; (i) S. van Wallandael and D. P. Rillema, *Coord. Chem. Rev.,* 1991, **111**, 297.

10 (a) M. D. Ward, *Coord. Chem. Rev.,* 2010, **254**, 2634; (b) M. D. Ward, *Coord. Chem. Rev.,* 2007, **251**, 1663; (c) S. Faulkner, L. S> Natrajan, W. S. Perry amd D. Sykes, *Dalton Trans.,* 2009, 3890.

11 (a) T. Lazarides, D. Sykes, S. Faulkner, A. Barbieri, and M. D. Ward, *Chem. Eur. J.,* 2008, **14**, 9389; (b) T. K. Ronson, T. Lazarides, H. Adams, S. J. A. Pope, D. Sykes, S.

Faulkner, S. J. Coles, M. B. Hursthouse, W. Clegg, R. W. Harrington and M. D. Ward, *Chem. Eur. J.,* 2006, **12**, 9299.

12 D. Sykes, S. C. Parker, I. V. Sazanovich, A. Stephenson, J. A. Weinstein and M. D. Ward, *Inorg. Chem.,* 2013, **52**, 10500.

13 D. Sykes, A. J. Cankut, N. Mohd Ali, A. Stephenson, S. J. P. Spall, S. C. Parker, J. A. Weinstein and M. D. Ward, *Dalton Trans.,* 2014, **43**, 6414.

14 (a) E. Baggaley, D.-K. Cao, D. Sykes, S. W. Botchway, J. A. Weinstein and M. D. Ward, *Chem. Eur. J.,* 2014, **20**, 8898; (b) A. Jana, E. Baggaley, A. Amoroso and M. D. Ward, *Chem. Commun.,* 2015, **51**, 8833.

15 (a) L. Flamigni, A. Barbieri, C. Sabatini, B. Ventura and F. Barigelletti, *Top. Curr. Chem.,* 2007, **281**, 143; (b) F. Spaenig, J.-H. Olivier, V. Prusakova, P. Retailleau, R. Ziessel and F. N. Castellano, *Inorg. Chem.,* 2011, **50**, 10859.

16 (a) K. S. Schanze, D. B. MacQueen, T. A. Perkins and L. A. Cabans, *Coord. Chem. Rev.,* 1991, **122**, 63; (b) H. Takeda, K. Koike, T. Morimoto, H. Inumaru and O. Ishitani, *Adv. Inorg. Chem.,* 2011, **63**, 137.

17 (a) M. Björling, G. Karlström and P. Linse, *J. Phys. Chem.,* 1991, **95**, 6706; (b) K.-J. Liu and J. L. Parsons, *Macromolecules,* 1969, **2**, 529; (c) F. Mueller-Plathe and W. F. van Gunsteren, *Macromolecules,* 1993, **27**, 6040; (d) R. Begum and H. Matsuura, *J. Chem. Soc., Faraday Trans.,* 1997, **93**, 3839; (e) G. Karlström and O. Engkvist, *ACS Symp. Ser.,* 1997, **680**, 16; (f) O. Engkvist and G. Karlström, *J. Chem. Phys.,* 1997, **106**, 2411; (g) N. Goutev, K. Ohno and H. Matsuura, *J. Phys. Chem. A,* 2000, **104**, 9226; (h) D. Bedrov, O. Borodin and G. D. Smith, *J. Phys. Chem. B,* 1998, **102**, 5683; (i) T. Ahlnas, G. Karlström and B. Lindman, *J. Phys. Chem.,* 1987, **91**, 4030.

18 (a) N. C. Fletcher, M. D. Ward, S. Encinas, N. Armaroli, L. Flamigni and F. Barigelletti, *Chem. Commun.,* 1999, 2089; (b) S. J. A. Pope, C. R. Rice, M. D. Ward, A. F. Morales, G. Accorsi, N. Armaroli and F. Barigelletti, *J. Chem Soc., Dalton Trans.,* 2001, 2228.

19 A. F. Morales, G. Accorsi, N. Armaroli, F. Barigelletti, S. J. A. Pope and M. D. Ward, *Inorg. Chem.,* 2002, **41**, 6711

20 (a) P. Coppo, E. A. Plummer and L. De Cola, *Chem. Commun.,* 2004, 1774; (b) F. O. Garces, K. A. King and R. J. Watts, *Inorg. Chem.,* 1988, **27**, 3464; (c) S. D. Sprouse, K. A. King, P. J. Spellane and R. J. Watts. *J. Am. Chem. Soc.,* 1984, **106**, 6647.

21 J. S. Fleming, K. L. V. Mann, C.-A. Carraz, E. Psillakis, J. C. Jeffery, J. A. McCleverty and M. D. Ward, *Angew. Chem., Int. Ed. Engl.,* 1998, **37**, 1279.

22 S. P. Argent, H. Adams, T. Riis-Johannessen, J. C. Jeffery, L. P. Harding, W. Clegg, R. W. Harrington and M. D. Ward, *Dalton Trans.,* 2006, 4996.

23 M. Arroyo, P. Gómez-Iglesias, N. Antón, R. García-Rodríguez, E. C. B. A. Alegria, A. J. L. Pombeiro, D. Miguel and F. Villafañe, *Dalton Trans.,* 2014, **43**, 4009.

24 G. M. Sheldrick, SADABS: A program for absorption correction with the Siemens SMART system, University of Göttingen, Germany, 2008.

25 G. M. Sheldrick, *Acta Crystallogr. Sect. A,* 2008, **64**, 112.

26 A. Spek, *J. Appl. Crystallogr.,* 2003, **36**, 7; P. van der Sluis and A. L. Spek, *Acta Crystallogr., Sect. A: Found. Crystallogr.,* 1990, **46**, 194.

Table 1. Crystal parameters, data collection and refinement details for the structures in this paper.

Complex	$[Ir(F_2ppy)_2(L^{oPh})](NO_3)$ •2.5MeCN•0.5MeOH	$\{[Ir(F_2ppy)_2(L^{mTol})](NO_3)\}_2$ •2MeCN•1.5Et_2O	$[Ir(F_2ppy)_2(L^{oPh})Re(CO)_3Cl](PF_6)$•MeCN
Abbreviation	Ir•L^{oPh}	Ir•L^{mTol}	Ir•L^{oPh}•Re
Formula	$C_{51.5}H_{41.5}F_4IrN_{11.5}O_{8.5}$	$C_{104}H_{89}F_8Ir_2N_{20}O_{7.5}$	$C_{51}H_{35}ClF_{10}IrN_9O_3PRe$
Molecular weight	1145.7	2275.35	1456.70
T, K	100(2)	100(2)	100(2)
Crystal system	Orthorhombic	Triclinic	Triclinic
Space group	*F*ddd	*P*-1	*P*-1
a, Å	25.9203(10)	11.7521(3)	12.999(3)
b, Å	31.5176(8)	12.3798(4)	14.835(3)
c, Å	46.0262(10)	34.4727(10)	16.683(3)
α, deg	90	86.2490(10)	70.940(9)
β, deg	90	85.957(2)	74.193(8)
γ, deg	90	71.7910(10)	75.254(8)
V, Å^3	37600.9(19)	4747.4(2)	2877.0(10)
Z	32	2	2
ρ, g cm^{-3}	1.619	1.592	1.682
Crystal size, mm^3	0.10 x 0.05 x 0.05	0.20 x 0.08 x 0.06	0.28 x 0.28 x 0.27
μ, mm^{-1}	2.916	2.886	4.566
Data, restraints, parameters	8391, 537, 649	16688, 1209, 1270	13119, 102, 750
Final *R*1, *wR*2[a]	0.0577, 0.1236	0.0776, 0.2386	0.0267, 0.0856

$[Ir(F_2ppy)_2(L^{mPh})Re(CO)_3Cl](NO_3)$•MeCN	$[Ir(F_2ppy)_2(L^{pPh})Re(CO)_3Cl](NO_3)$•MeCN	$[Ir(F_2ppy)_2(L^{nap})Re(CO)_3Cl](NO_3)$•2MeCN
Ir•L^{mPh}•Re	Ir•L^{pPh}•Re	Ir•L^{nap}•Re
$C_{51}H_{35}ClF_4IrN_{10}O_6Re$	$C_{51}H_{35}ClF_4IrN_{10}O_6Re$	$C_{57}H_{40}ClF_4IrN_{11}O_6Re$
1373.74	1373.74	1464.85
100(2)	100(2)	100(2)
Triclinic	Monoclinic	Monoclinic
P-1	*P*2/n	*C*2/c
10.8363(5)	17.2876(10)	22.5334(14)
12.5992(7)	13.6694(9)	27.4539(14)
18.0874(9)	24.8368(14)	20.7788(12)
77.485(3)	90	90
89.899(3)	94.513(2)	122.123(3)
89.764(3)	90	90
2410.7(2)	5851.0(6)	10886.5(11)
2	4	8
1.892	1.559	1.787
0.21 x 0.11 x 0.07	0.10 x 0.06 x 0.06	0.12 x 0.08 x 0.06
5.399	4.449	4.789
8607, 0, 668	13450, 9, 632	9711, 535, 613
0.0312, 0.0864	0.0473, 0.1091	0.0416, 0.1055

[a] The value of *R*1 is based on 'observed' data with $I > 2\sigma(I)$; the value of w*R*2 is based on all data.

Table 2. Metal-ligand bond distances, and Ir•••Re separations (both in Å), for the structurally characterised complexes.

Ir•L^{oPh}

Ir(1)-C(26B)	2.009(7)	Ir(1)-N(11C)	2.047(6)
Ir(1)-C(26C)	2.013(8)	Ir(1)-N(11A)	2.146(6)
Ir(1)-N(11B)	2.043(6)	Ir(1)-N(22A)	2.154(6)

Ir•L^{mTol}

Ir(1)-C(26B)	2.002(10)	Ir(2)-C(26E)	2.007(11)
Ir(1)-C(26C)	2.011(12)	Ir(2)-N(11F)	2.036(9)
Ir(1)-N(11C)	2.032(9)	Ir(2)-N(11E)	2.043(9)
Ir(1)-N(11B)	2.057(10)	Ir(2)-C(26F)	2.051(11)
Ir(1)-N(22A)	2.141(8)	Ir(2)-N(22D)	2.164(9)
Ir(1)-N(11A)	2.148(9)	Ir(2)-N(11D)	2.191(8)

Ir•L^{oPh}•Re

Ir(1)-C(26B)	2.012(4)	Re(2)-C(31D)	1.910(4)
Ir(1)-C(26C)	2.013(4)	Re(2)-C(21D)	1.930(4)
Ir(1)-N(11B)	2.047(3)	Re(2)-C(11D)	1.954(5)
Ir(1)-N(11C)	2.053(3)	Re(2)-N(42A)	2.174(3)
Ir(1)-N(22A)	2.166(3)	Re(2)-N(31A)	2.199(3)
Ir(1)-N(11A)	2.168(3)	Re(2)-Cl(1)	2.4824(12)
Ir(1)-Re(2)	8.84		

Ir•L^{mPh}•Re

Ir(1)-C(26B)	2.005(7)	Re(2)-C(21D)	1.909(8)
Ir(1)-C(26C)	2.013(7)	Re(2)-C(31D)	1.917(7)
Ir(1)-N(11C)	2.046(5)	Re(2)-C(11D)	1.977(10)
Ir(1)-N(11B)	2.048(5)	Re(2)-N(42A)	2.175(5)
Ir(1)-N(22A)	2.150(5)	Re(2)-N(31A)	2.205(5)
Ir(1)-N(11A)	2.169(5)	Re(2)-Cl(1)	2.487(2)
Ir(1)-Re(2)	9.81		

Ir•L^{pPh}•Re

Ir(1)-C(26C)	1.985(6)	Re(1)-C(21D)	1.907(6)
Ir(1)-C(26B)	2.002(6)	Re(1)-C(11D)	1.921(7)
Ir(1)-N(11B)	2.047(5)	Re(1)-C(31D)	1.943(7)
Ir(1)-N(11C)	2.054(5)	Re(1)-N(42A)	2.177(5)
Ir(1)-N(22A)	2.127(5)	Re(1)-N(31A)	2.196(5)
Ir(1)-N(11A)	2.152(5)	Re(1)-Cl(1)	2.4770(15)
Ir(1)-Re(2)	9.75		

Ir•L^{nap}•Re

Ir(1)-C(26B)	2.020(3)	Re(2)-C(11D)	1.902(8)
Ir(1)-C(26C)	2.025(3)	Re(2)-C(31D)	1.915(9)
Ir(1)-N(11B)	2.035(3)	Re(2)-C(21D)	1.916(9)
Ir(1)-N(11C)	2.038(3)	Re(2)-N(42A)	2.136(3)
Ir(1)-N(22A)	2.109(3)	Re(2)-N(31A)	2.196(3)
Ir(1)-N(11A)	2.174(3)	Re(2)-Cl(1)	2.470(2)
Ir(1)-Re(2)	9.73		

Table 3. UV/Vis absorption spectra for the new complexes[a]

Complex	λ_{max} / nm (10^{-3} ε / M^{-1} cm^{-1})
Ir•L^{oPh}	360 (5.4), 313 (16), 280 (44), 250 (66)
Ir•L^{mTol}	360 (5.3), 313 (16), 280 (38), 250 (59)
Ir•L^{PEG}	360 (5.7), 315 (17), 280 (40), 250 (59)
Re•L^{Me}	337 (4.9), 305 (sh), 295(13), 280(12), 250 (sh), 220 (29)
Ir•L^{but}•Re	360 (7.0), 295(34), 246(63)
Ir•L^{naph}•Re	360 (8.0), 290 (53), 278 (53), 246 (72)
Ir•L^{mTol}•Re	360 (8.3), 295 (39), 246 (69)
Ir•L^{oPh}•Re	360 (7.5), 295 (37), 246 (67)
Ir•L^{mPh}•Re	360 (7.0), 295 (33), 246 (62)
Ir•L^{pPh}•Re	360 (7.2), 295 (35), 246 (61)
Ir•L^{PEG}•Re[b]	360 (11), 295 (46), 280 (54), 246 (780)

a All spectra recorded in MeCN unless stated otherwise
b Measured in CH_2Cl_2

Table 4. Luminescence lifetimes for complexes in degassed MeCN at room temperature.

Complex	Rise-time	Decay
Ir•L^{oPh}	*n/a*	4.4 µs[a]
Ir•L^{mPh}	*n/a*	4.2 µs[a]
Ir•L^{pPh}	*n/a*	4.4 µs[a]
Ir•L^{but}	*n/a*	3.6 µs[a]
Ir•L^{mTol}	*n/a*	4.5 µs[a]
Ir•L^{PEG}	*n/a*	3.3 µs[a]
Ir•L^{but}•Re	13 ns[b]	259 ns[c]
s	126 ns[b]	378 ns[c]
Ir•L^{oPh}•Re	94 ns[b]	328 ns[c]
Ir•L^{mPh}•Re	92 ns[b]	320 ns[c]
Ir•L^{pPh}•Re	108 ns[b]	378 ns[c]
Ir•L^{PEG}•Re	35 ns[b]	265 ns[c]

a Ir-based luminescence decay
b Re-based rise-time due to Ir→Re energy-transfer
c Re-based luminescence decay

Figure captions

Fig. 1 Summary of the ligands used in this paper.

Fig. 2 A view of the complex cation in the crystal structure of Ir•L^{oPh}

Fig. 3 A view of the complex cation in the crystal structure of Ir•L^{mTol}

Fig. 4 Parts of the NMR spectra of (a) Ir•L^{oPh} and (b) Ir•L^{oPh}•Re, showing how in the latter case the presence of a mixture of diastereoisomers results in splitting of signals. The expansions of the most highly shifted signal in each case show how a doublet for Ir•L^{oPh} (a pyridyl H^6 proton) gives the appearance of a 'dd' signal in Ir•L^{oPh}•Re when it is in fact two overlapping half-intensity doublets, one for each diastereoisomer. The signals labelled * in the spectrum of Ir•L^{oPh}•Re are half-intensity signals arising from one diastereoisomer, with the partner signal for the other diastereoisomer obscured by overlapping signals elsewhere in the spectrum.

Fig. 5 A view of the complex cation in the crystal structure of Ir•L^{oPh}•Re

Fig. 6 A view of the complex cation in the crystal structure of Ir•L^{mPh}•Re

Fig. 7 A view of the complex cation in the crystal structure of Ir•L^{pPh}•Re

Fig. 8 A view of the complex cation in the crystal structure of Ir•L^{naph}•Re

Fig. 9 UV/Vis absorption spectrum and (inset) steady-state luminescence spectrum of Ir•L^{oPh} in MeCN at RT.

Fig. 10 (a) UV/Vis absorption spectrum of Ir•L^{pPh}•Re in MeCN at RT. (b) Luminescence spectra of Ir•L^{oPh}•Re (red), Ir•L^{mTol}•Re (green) and Ir•L^{but}•Re (blue) in air-equilibrated MeCN (λ_{exc} = 360 nm) at RT. Spectra have been normalised to the highest-energy feature at 452 nm.

Fig. 11 Time-resolved emission intensity (in the range 550 – 600 nm) of Ir•L^{but}•Re (red) and Ir•L^{mTol}•Re (blue), measured in degassed MeCN at RT, showing the rise-time associated with Ir→Re energy-transfer and sensitisation of the Re-based luminescence component (λ_{exc} = 400 nm).

Fig. 12 Absorption spectrum of Re•L^{Me} (black) and luminescence spectrum of Ir•L^{pPh} (red), illustrating the very small region of overlap (highlighted by the blue arrow) which makes Dexter energy-transfer possible.

Fig. 13 *Main picture:* Overlaid luminescence spectra of mononuclear Ir•L^{PEG} (black line) in MeCN, and dinuclear Ir•L^{PEG}•Re in a range of solvents showing different extents of Ir→Re PEnT according to solvent polarity. In order of increasing polarity these are CH_2Cl_2 (red), MeCN (blue), MeOH (orange), MeCN(90%)/water(10%) (green), MeCN(80%)/water(20%) (purple), water (pale blue). Spectra have been normalised to the highest-energy feature at 452 nm. *Inset:* difference between the black (Ir•L^{PEG} in MeCN) and red (Ir•L^{PEG}•Re in CH_2Cl_2) luminescence spectra from the main image, showing the additional sensitised Re-based emission component which exactly matches the luminescence spectrum profile of Re•L^{Me}.

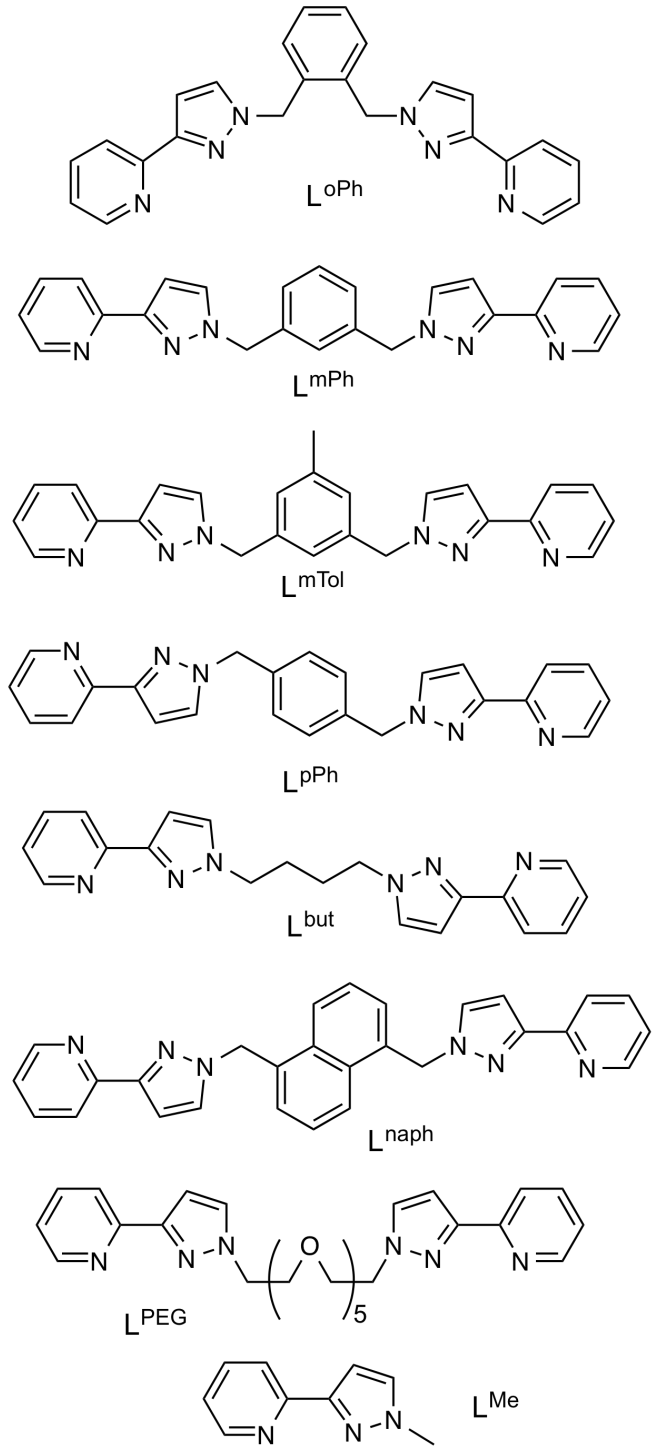

Figure 1

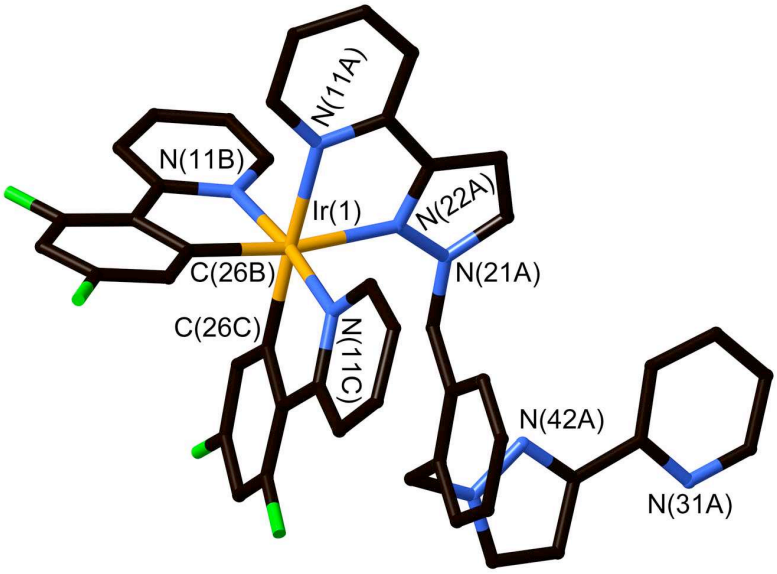

Figure 2

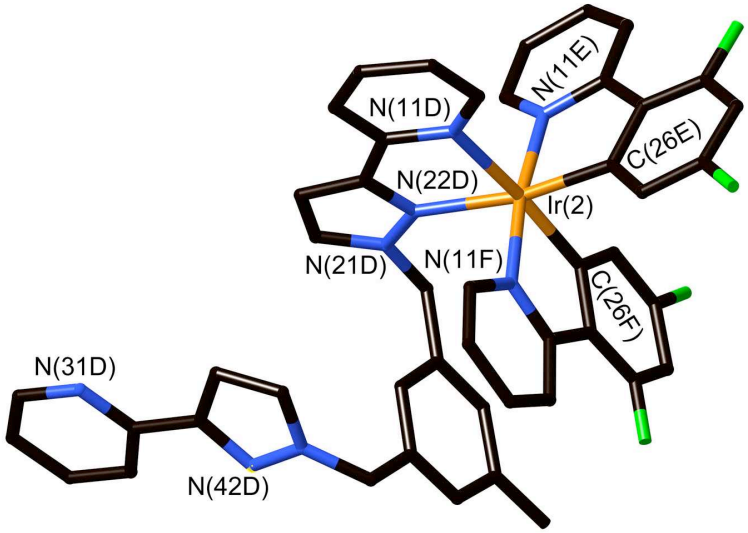

Figure 3

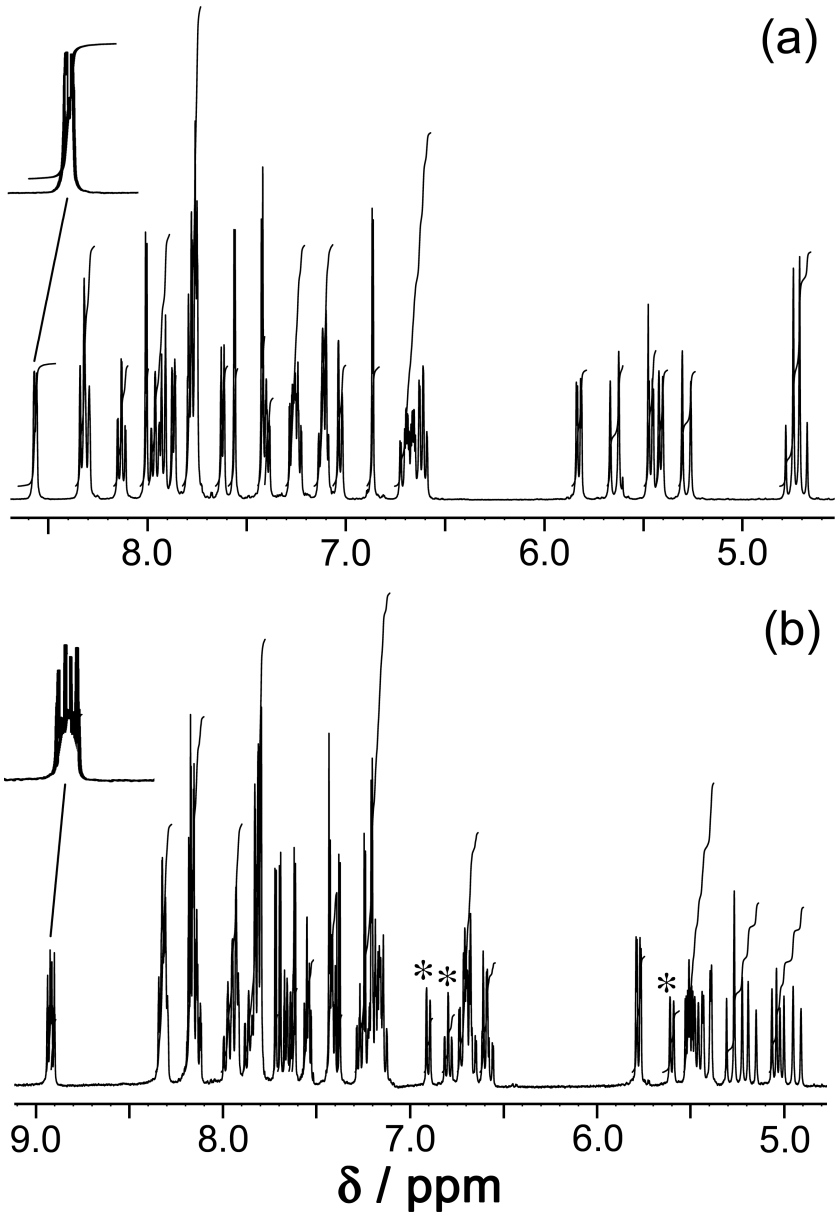

Figure 4

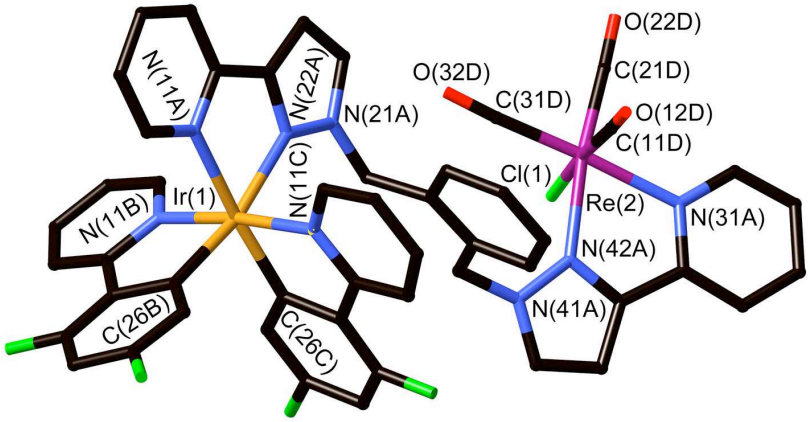

Figure 5

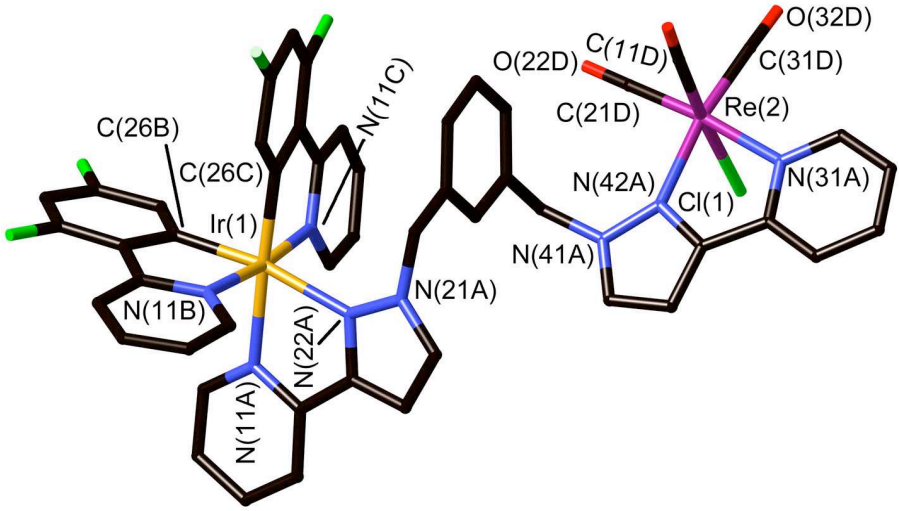

Figure 6

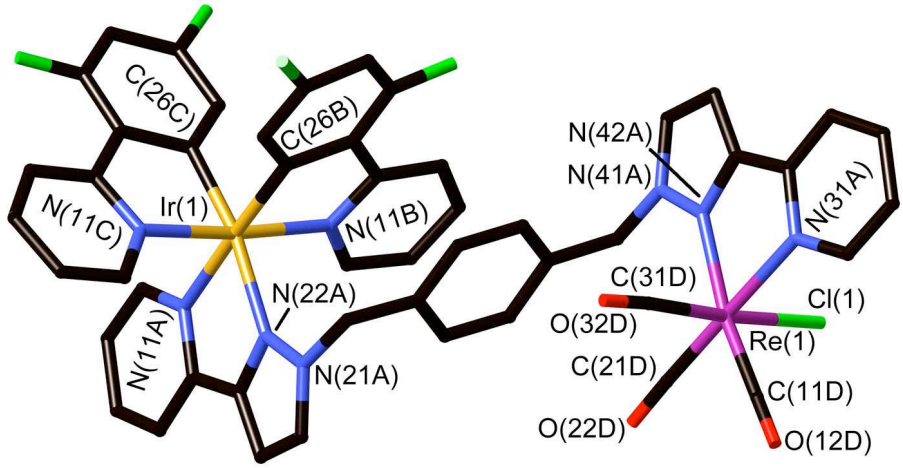

Figure 7

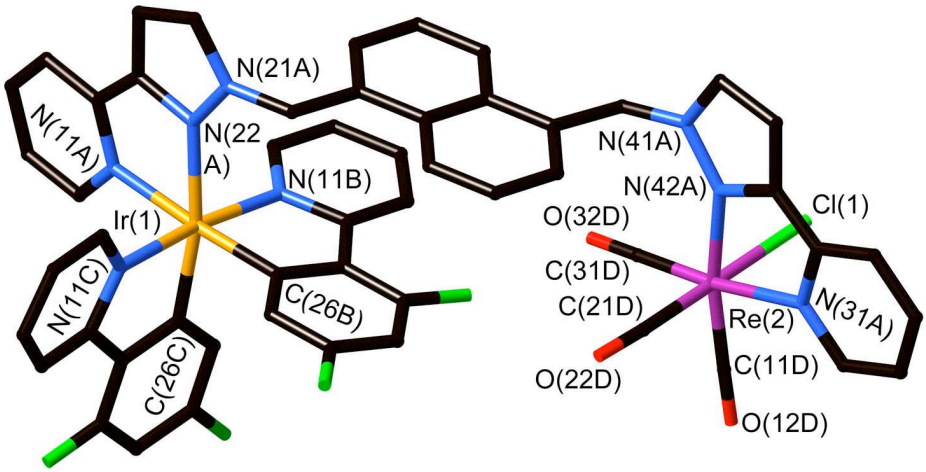

Figure 8

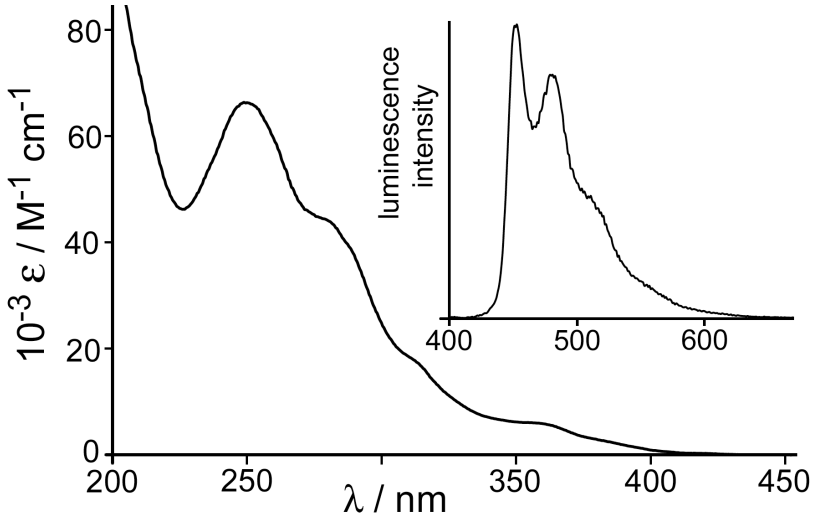

Figure 9

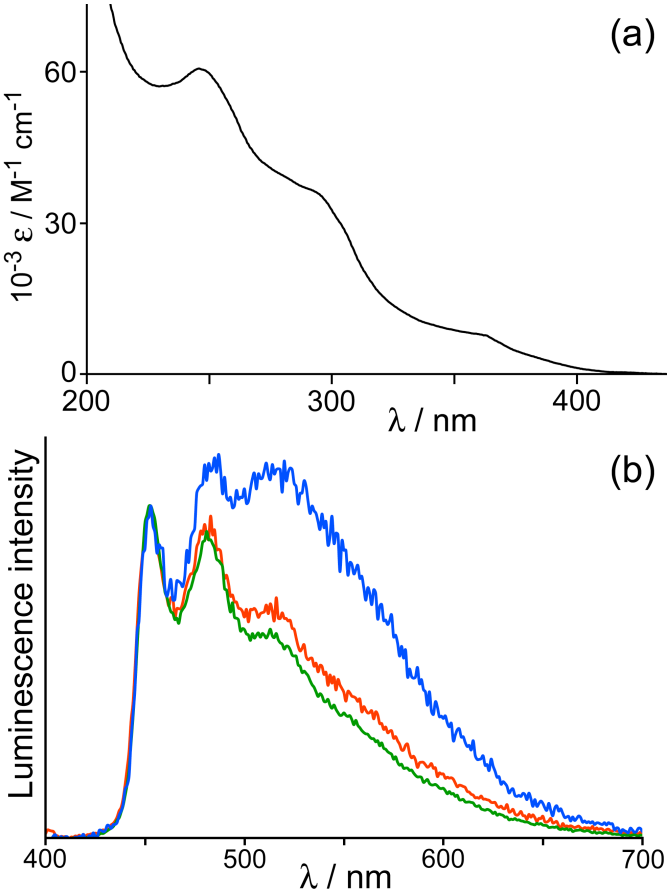

Figure 10

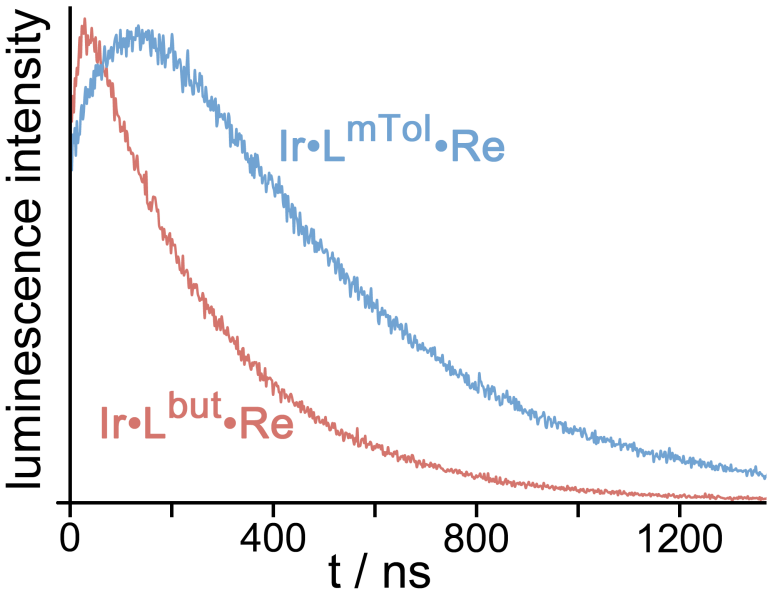

Figure 11

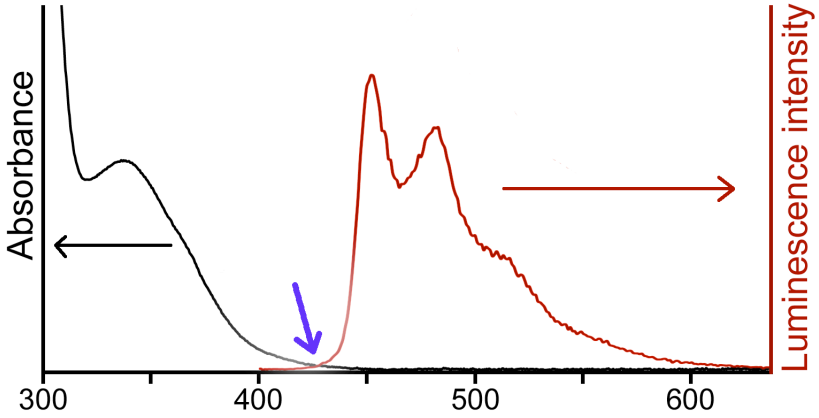

Figure 12

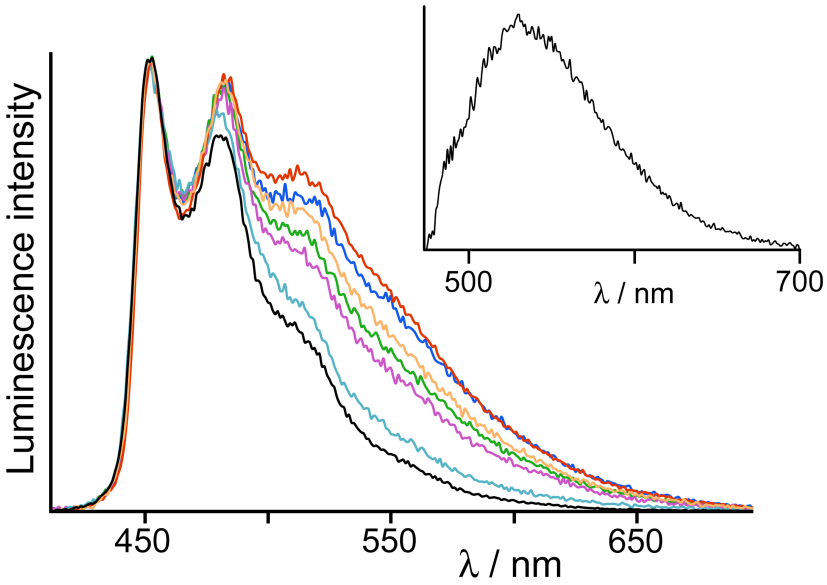

Figure 13

Synthesis and photophysical properties of Ir(III)/Re(I) dyads: control of Ir→Re photoinduced energy transfer

Suad T. Saad, Alexander J. Metherell, Elizabeth Baggaley and Michael D. Ward*

Graphical abstract for Table of Contents

The extent of Ir→Re photoinduced energy transfer in Ir(III)/Re(I) dyads can be controlled using a solvent-sensitive conformationally flexible bridging ligand.